

Nitrogen-doped TiO₂ nanotube array films with enhanced photocatalytic activity under various light sources

Yue-Kun Lai^{a,b}, Jian-Ying Huang^c, Hui-Fang Zhang^a, Vishnu-Priya Subramaniam^b, Yu-Xin Tang^b, Dang-Guo Gong^b, Latha Sundar^b, Lan Sun^a, Zhong Chen^b, Chang-Jian Lin^{a,*}

^a State Key Laboratory of Physical Chemistry of Solid Surfaces, and College of Chemistry and Chemical Engineering, Xiamen University, Xiamen 361005, China

^b School of Materials Science and Engineering, Nanyang Technological University, 50 Nanyang Avenue, Singapore 639798, Singapore

^c Fujian Institute of Research on the Structure of Matter, Chinese Academy of Sciences, Fuzhou 350002, China

ARTICLE INFO

Article history:

Received 17 March 2010
Received in revised form 28 August 2010
Accepted 31 August 2010
Available online 15 September 2010

Keywords:

TiO₂ nanotube array
Nitrogen-doping
Visible light activity
Methyl orange
Intermediate

ABSTRACT

Highly ordered nitrogen-doped titanium dioxide (N-doped TiO₂) nanotube array films with enhanced photocatalytic activity were fabricated by electrochemical anodization, followed by a wet immersion and annealing post-treatment. The morphology, structure and composition of the N-doped TiO₂ nanotube array films were investigated by FESEM, XPS, UV-vis and XRD. The effect of annealing temperature on the morphology, structures, photoelectrochemical property and photo-absorption of the N-doped TiO₂ nanotube array films was investigated. Liquid chromatography and mass spectrometry were applied to the analysis of the intermediates coming from the photocatalytic degradation of MO. The experimental results showed that there were four primary intermediates existing in the photocatalytic reaction. Compared with the pure TiO₂ nanotube array film, the N-doped TiO₂ nanotubes exhibited higher photocatalytic activity in degrading methyl orange into non-toxic inorganic products under both UV and simulated sunlight irradiation.

Crown Copyright © 2010 Published by Elsevier B.V. All rights reserved.

1. Introduction

Since the discovery of water photolysis on TiO₂ electrode by Fujishima and Honda [1] in 1972, TiO₂ became one of the most widely researched materials for use in solar cells [2,3], pollutant degradation [4–6], photolysis of water [7,8], gas sensor [9,10] and bio-applications [11,12] due to its unique and favorable physico-chemical properties. However, the anatase TiO₂ material cannot efficiently utilize visible light ($\lambda > 380$ nm) of the solar energy because of its comparably large band gap. To overcome this problem, considerable efforts have been taken to narrow the band gap. Doping with different types of transition metal cations [13–15], surface modification with noble metal [16–19], as well as doping with nonmetal anions [20–41] have been explored in an effort to increase the visible light absorption or suppress the recombination of photogenerated carries.

Asahi et al. reported a visible light active TiO_{2-x}N_x film by sputtering the TiO₂ target in a N₂/Ar gas mixture, which attracted a great attention of N-doped TiO₂ as a visible light photocatalyst [20]. The common approaches to form N-doped TiO₂ photocatalyst include sputtering of TiO₂ targets in N₂ mixture gas [31,32], annealing

TiO₂ or Ti-compounds under ammonia gas [33–37], ion implantation and thermal treatment [38,39], and hydrolysis of N-containing solutions [40,41].

Although N-doped TiO₂ has been widely fabricated and studied for the photocatalysis under visible light irradiation, most of the work uses either powders or thin compact films. In the present work, we investigate the N-doped TiO₂ nanotube array film prepared by treating TiO₂ nanotube array film with ammonia solution. This method avoided the use of hazardous ammonia gas, or laborious ion implantation process. Moreover, to our knowledge, there are so far few reports about the effect of N-doping and annealing temperature on the photocatalytic performance of TiO₂ photocatalyst under different light sources. In the current work, high-pressure mercury lamp and tungsten-halogen lamp light sources have been used. Photocatalytic activity of doped and undoped TiO₂ nanotube films was investigated.

2. Experimental

2.1. Preparation of N-doped TiO₂ nanotube arrays

Highly ordered TiO₂ nanotube arrays with a tube length about 350 nm were grown from Ti sheets (>99.6% purity) via electrochemical anodization in 0.5% HF electrolyte with Pt counter electrode under 20 V for 20 min as previously described in the literature

* Corresponding author.

E-mail address: cjlin@xmu.edu.cn (C.-J. Lin).

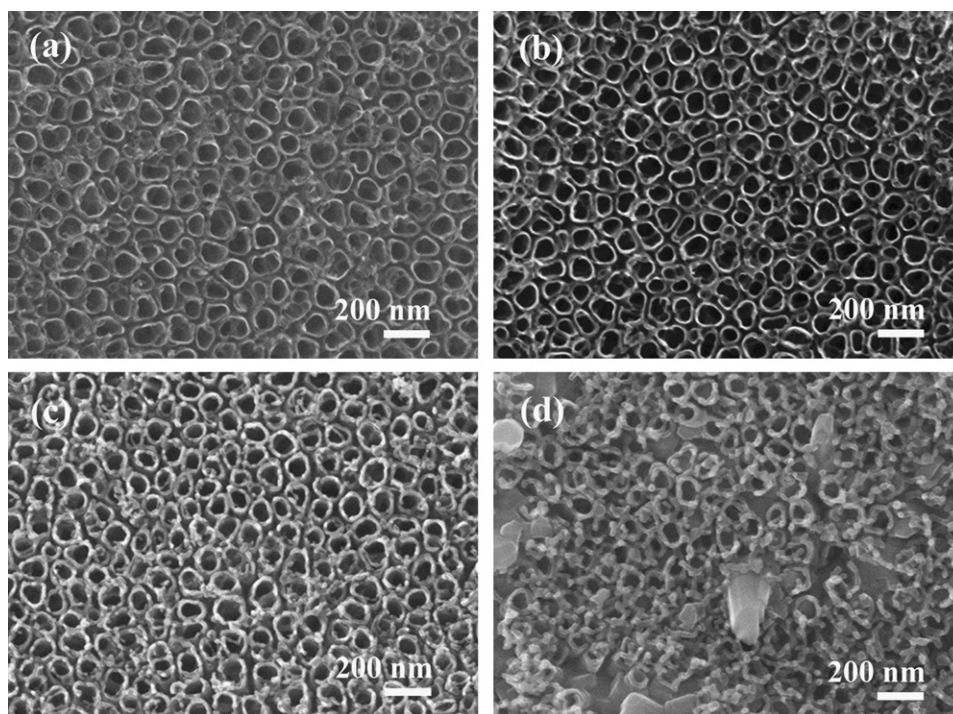


Fig. 1. SEM top-view images of (a) TiO₂ nanotube array annealed at 450 °C, N-doped TiO₂ nanotube arrays annealed at various temperatures (b) 450 °C, (c) 600 °C, and (d) 700 °C.

[42,43]. The as-prepared samples were immersed in 1 M NH₃·H₂O solution for 10 h and annealed in a muffle furnace under ambient atmosphere for 2 h to obtain N-doped TiO₂ nanotube array electrode with crystalline phase.

2.2. Characterization of N-doped TiO₂ nanotube arrays

The morphologies of the prepared samples were observed using a field emission scanning electron microscope (FESEM, LEO-1530) and their crystalline phase was identified using an X-ray diffractometer (Philips, Panalytical X'pert, Cu K α radiation). The surface chemical composition of samples was analyzed by X-ray photoelectron spectroscopy (XPS, PHI Quantum 2000) with Al K α radiation source. All the binding energies were referenced to the C1s peak at 284.8 eV of surface adventitious carbon. The absorption properties of the samples were recorded using a diffuse reflectance UV-vis spectrometer (Varian, Cary 5000) with wavelength range of 300–650 nm.

2.3. Photoelectrochemical and photocatalytic measurements

Photoelectrochemical measurements were carried out in 0.1 M Na₂SO₄ solution using an LHX 150 Xe lamp, a SBP 300 grating spectrometer, and an electrochemical cell with a quartz window. The generated photocurrent signal was collected by a lock-in amplifier (5210, EG and G, PAR Co., USA) with a light chopper at zero bias with a step of 5 nm in the range of 300–600 nm. The reproducibility was checked by repeating the measurement at least three times and the average value is taken as the reported photocurrent. Electrochemical impedance spectroscopy (EIS) spectra were measured by applying an AC voltage of 10 mV amplitude within the frequency range of 10⁵–10⁻² Hz in 0.1 mol L⁻¹ Na₂SO₄ solution.

For the photocatalytic degradation experiments, methyl orange (MO) was chosen as a target compound. The detail processes are similar with the ones previously described in the literature [44,45]. The initial concentration of the dye was 20 mg/L and the pH value of the MO solution (pH = 3.0) was adjusted with H₂SO₄. The quartz

glass reactor was equipped with a water jacket to control the temperature. The photo-irradiation was performed with a 200 W high-pressure mercury lamp emitting at a wavelength of 365 nm as the UV light source and 500 W tungsten-halogen lamp was used to produce the simulated sunlight. Before the photocatalytic degradation, the photocatalyst (1.0 cm \times 1.5 cm) was soaked in 30 mL MO solution for 30 min to establish the adsorption/desorption equilibrium. The solution periodically taken from the reactor was analyzed with a UV-vis spectrophotometer (Shimadzu UV-2100, Japan). The analytical wavelength selected for optical absorbance measurement was 508 nm. The blank test was also carried out by irradiating MO homogeneous solution without TiO₂ photocatalyst for checking the self-photolysis of MO.

Samples were taken from the reaction vessels and filtered through a 0.2 μ m cellulose membrane filter. HPLC analysis was carried out using Agilent 1200 series HPLC with UV DAD detector. RP-C18 column (Agilent Zorbax XDB C-18, 250 mm \times 4.6 mm; 5 mm particles) was used to separate the degradation products present in the reaction mixture. Acetonitrile/Ammonium acetate (10 mM, pH = 6.6) were used as a mobile phase with 24/76 (v/v) and 0.8 ml min⁻¹ as a flow rate. The products were detected by UV-vis diode array detector. MALDI-TOF mass spectra were recorded on a Shimadzu Biotech Axima ToF² MS instrument equipped with the delayed extraction option. Ionisation (negative) was achieved using a N₂ laser source (337 nm). The mass spectrometer was operated in a reflectron negative mode, and for this operation mode the instrument was calibrated using small-cal-mix samples. The analyses were done without aid of any matrix.

3. Results and discussion

3.1. Characterization of N-doped TiO₂ nanotube array films

Fig. 1 shows top-view SEM images of the as-prepared TiO₂ nanotube array annealed at 450 °C (Fig. 1(a)) and the N-doped TiO₂ nanotube array (Fig. 1(b)–(d)) annealed at 450, 600 and 700 °C for

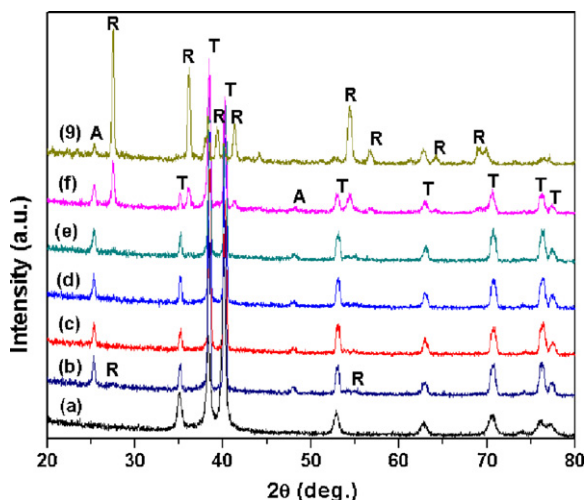


Fig. 2. XRD patterns of the pure TiO_2 nanotube array film and N-doped TiO_2 nanotube array films annealed at temperatures ranging from 300 to 700 °C. Pure TiO_2 nanotube samples: (a) before annealing, (b) 450 °C; N-doped TiO_2 nanotube samples: (c) 300 °C, (d) 450 °C, (e) 500 °C, (f) 600 °C, and (g) 700 °C. A, R, and T represent anatase, rutile and titanium, respectively.

2 h. Both N-doped and pure TiO_2 film annealed at 450 °C show similar morphology to the as-prepared sample. This indicates low temperatures have no great effect on surface morphology and architecture of the TiO_2 nanotube array. The nanotube arrays have an average tube diameter around 80 nm and a wall thickness of about 15 nm. When annealed at 600 °C, the diameter of the N-doped TiO_2 nanotube slightly decreases and the wall thickness increases, indicating the obvious anatase crystal growth and rutile phase transition of TiO_2 nanotube. When annealing temperature increased to 700 °C, some part of the nanotube array architecture collapsed, this is ascribed to high temperature and phase transition heat lead to the rapid grain growth within the thin tube wall and in the underlying titanium foil [46–48].

It is well known that surface morphology change is close related to crystal growth and phase transformation. Therefore, XRD was investigated to analyze the effect phase transformation on the change of surface morphology and TiO_2 nanotube structures. Fig. 2 shows the XRD patterns for the pure titania nanotube film and N-doped titania nanotube films under various annealing temperatures. The as-grown TiO_2 thin film (curve a) exhibits an amorphous structure except for the existence of typical diffraction peaks of metallic titanium [49,50]. Hence, the annealing process is necessary to transfer the amorphous TiO_2 film into a well-crystallized anatase phase. For samples annealed at 300 °C for 2 h (curve c), two weak diffraction peaks appeared at 25.4° and 48.1°, in well accordance with the (101) and (200) peaks of anatase titania, indicating the initial formation of tiny crystalline anatase phase, whereas no evidence of the existence of rutile phase is observed. Further increasing the annealing temperature, the strength of these two anatase peaks also increases. Moreover, the pure TiO_2 nanotube samples have more obvious rutile peaks (curve b) than that of N- TiO_2 sample (curve d) under 450 °C heat treatment. This indicates that the incorporation N-dopants into the TiO_2 lattice via O–Ti–N bonding can suppress the anatase–rutile phase transition to enhance the thermal stability of anatase owing to the strong crystal distortion force [51,52]. In addition, the presence of porous nanotube structures and the N-doping might inhibit the migration and the arrangement of Ti and O atoms to form rutile during high temperature calcinations [48,53]. When annealed at 500 °C (curve e), a small peak appeared at 27.61°, indicating the starting transition of anatase phase to more stable rutile phase. As the temperature rose (curves f and g), the diffraction peak of rutile phase became stronger

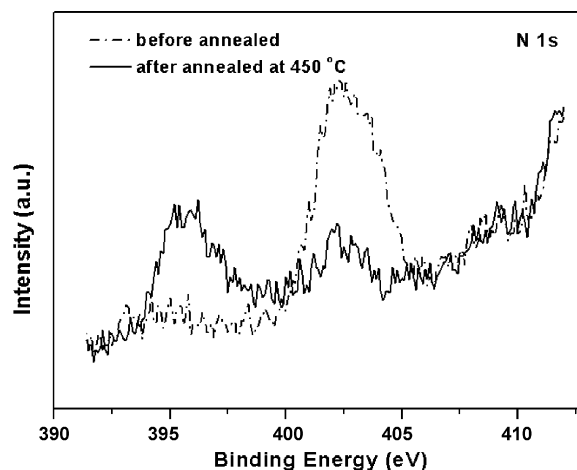


Fig. 3. The high-resolution spectra of N1s region of the before (dotted line) and after 450 °C annealing for 2 h (solid line).

and the diffraction peaks of anatase phase nearly disappeared at 700 °C.

The high resolution spectrum of XPS was used to identify the nitrogen elements present on the TiO_2 nanotube arrays. Fig. 3 shows the high resolution XPS N 1s core level spectra of ammonia treated TiO_2 nanotube array film before and after annealing. It is cleared that only a strong N species peak at around 402.0 ± 0.2 eV can be observed before heat treatment (dotted line). The intensity became weak after annealing, indicating the N-state is just molecularly chemisorbed on surface of TiO_2 in the soaking process. However, a new and strong peak appeared at 395.9 ± 0.2 eV can be assigned to N^{3-} substituting for O^{2-} at anion site [54]. This indicates that the heat treatment has led to the change from adsorbed state to the substituting state in TiO_2 .

The UV-vis diffuse reflection spectra of pure TiO_2 nanotube array film and N-doped TiO_2 nanotube array films by the different annealing temperature are displayed in Fig. 4. It is apparent that the absorbance of all the N-doped TiO_2 nanotube array films are stronger than that of the pure TiO_2 nanotube array film at wavelengths greater than 400 nm. Moreover, the absorption edges of the N-doped TiO_2 nanotube array films show a slight red-shift. This red-shift of the absorption edge is related to the N-doping in the intrinsic band gap of TiO_2 and the interaction between N 2p and O 2p orbit. The broad absorption peaks were identified

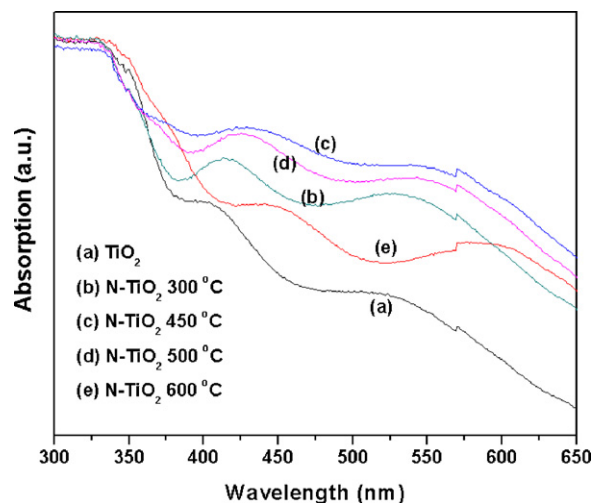


Fig. 4. UV-vis absorption spectra of TiO_2 nanotube arrays under different annealing temperatures.

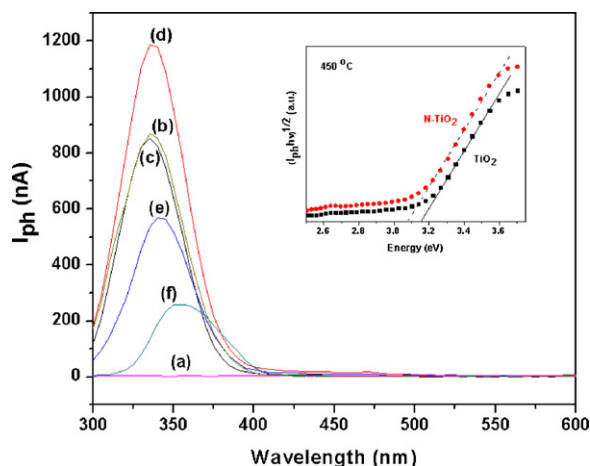


Fig. 5. Photocurrent spectra of as-prepared pure TiO₂ nanotube array film without annealing (a), pure TiO₂ nanotube array annealed at 450 °C (b) and N-doped TiO₂ nanotube array films annealed at different temperatures. (c) 300 °C; (d) 450 °C; (e) 500 °C; (f) 600 °C. The inset shows the $(I_{ph} \times hv)^{1/2}$ versus hv plots of the 450 °C annealed pure and N-doped TiO₂ nanotube array film.

to be the sub-band gap states of the TiO₂ nanotube array due to its special nanotube structures [55,56]. The doped TiO₂ nanotube array firstly increases the UV-vis absorption below 450 °C. It shows that the calcined N-doped TiO₂ nanotube array achieved the great absorbance at 450 °C. The absorbance decreases with the further increasing annealing temperature from 450 to 700 °C. The reason may be due to the phase transformation from the anatase to rutile which combined with the rapid growth of crystallites and decrease of the surface area of the TiO₂ nanotube array.

3.2. Photoelectrochemical property

Fig. 5 shows the photocurrent versus wavelength plots for the different annealing temperature of N-doped TiO₂ nanotube array films. The photocurrent first increased significantly with the annealing temperature of the N-doped nanotube array film, and a maximum was observed for the sample annealed at 450 °C. This is due to the phase change from amorphous to anatase according to the XRD results. The increasing anatase phase ratio of the N-doped TiO₂ nanotube array films may enhance the separation and transferring efficient of the photo-generated carriers, resulting in an increase in photogenerated current [57,58]. Further increasing the annealing temperature leads to a decline of photocurrent intensity, and a shift of photocurrent peak to higher wavelength. When annealed at temperatures higher than 450 °C, the anatase

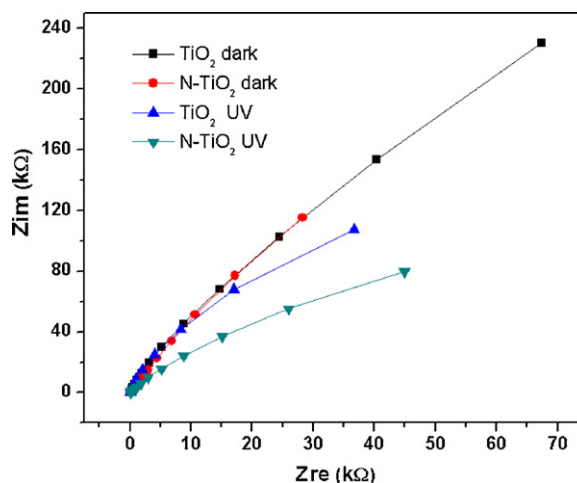


Fig. 6. Nyquist plots of the 450 °C annealed TiO₂ nanotube array electrodes in dark and under UV light illumination.

phase started to change to the more stable rutile phase with a lower band gap. This transition process is accompanied by thicker nanotube wall or even the destruction of the uniform nanotube array structures. These situations would deteriorate the separation and transferring of photogenerated carriers. For instance, comparing the photocurrent of sample annealed by 450 °C (curve d) and 600 °C (curve f), a difference of about six times was observed.

The inset figure shows the corresponding $(I_{ph} \times hv)^{1/2}$ versus hv plots of the pure TiO₂ and N-doped TiO₂ samples which were used for the determination of the indirect band gap energy of the TiO₂ films. Clearly, the band gap energy of the 450 °C annealed N-doped TiO₂ nanotube array sample is approximately 3.07 ± 0.05 eV, which is lower than that of the pure TiO₂ nanotube array sample (3.16 ± 0.05 eV) and the typical value reported for anatase phase [59,60]. This is also in accordance with the above UV-vis absorption result.

Fig. 6 gives the typical Nyquist plots of EIS spectra for TiO₂ nanotube array electrodes with or without UV light irradiation. The impedance arc radius of electrodes in the dark were much bigger than that under UV light irradiation, which indicated that there were few electrons across the TiO₂-electrolyte interfaces in dark. While under the UV light illumination, the arc radius of the N-doped TiO₂ nanotube array electrode is smaller than that of the un-doped electrode. This demonstrated that the N-doped nanotube array electrode displayed greater separation efficiency of photogenerated electron-hole pairs and faster charge transfer than that of the pure TiO₂ nanotube film at the solid-liquid interface. Therefore,

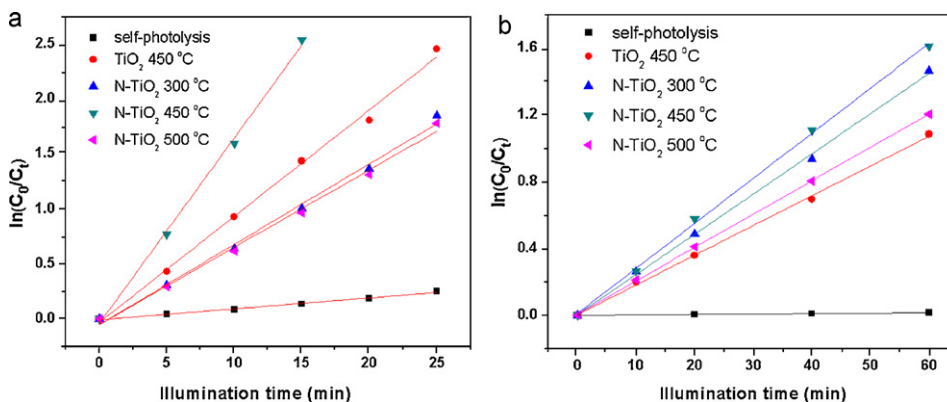
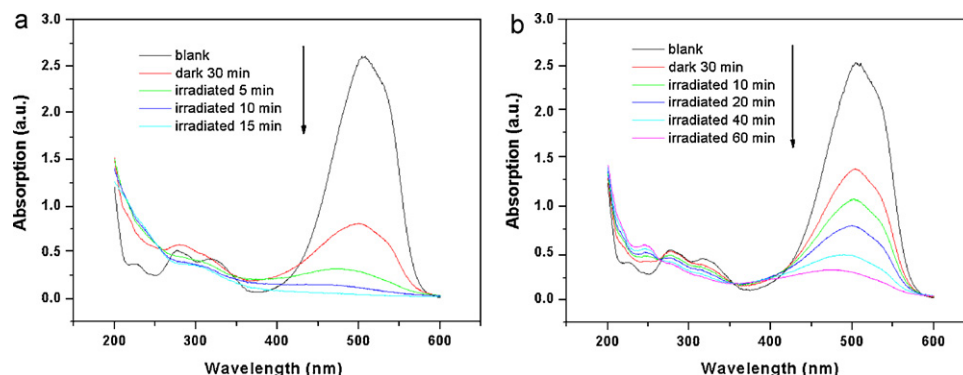


Fig. 7. Comparison of photocatalytic degradation rates of MO for pure TiO₂ and N-doped TiO₂ nanotube array films with different annealing temperatures under high-pressure mercury lamp illumination (a) and tungsten-halogen lamp illumination (b).

Table 1Effect of the annealing temperature of N-doped TiO₂ nanotube array film on the photocatalytic degradation first-order rate constant *k* under different light sources.

Photocatalyst	Self-photolysis	TiO ₂	N-TiO ₂	N-TiO ₂	N-TiO ₂
		450 °C	300 °C	450 °C	500 °C
Under high pressure mercury lamp illumination					
Apparent rate constant <i>k</i> (min ⁻¹)	0.0100	0.0967	0.0732	0.1690	0.0704
Correlation coefficient <i>R</i> ²	0.9923	0.9952	0.9927	0.9966	0.9926
Under tungsten–halogen lamp illumination					
Apparent rate constant <i>k</i> (min ⁻¹)	–	0.0178	0.0241	0.027	0.0200
Correlation coefficient <i>R</i> ²	–	0.9983	0.9984	0.9986	0.9998

**Fig. 8.** UV-visible spectra of MO at different time intervals under high-pressure mercury lamp illumination (a), under tungsten–halogen lamp illumination (b).

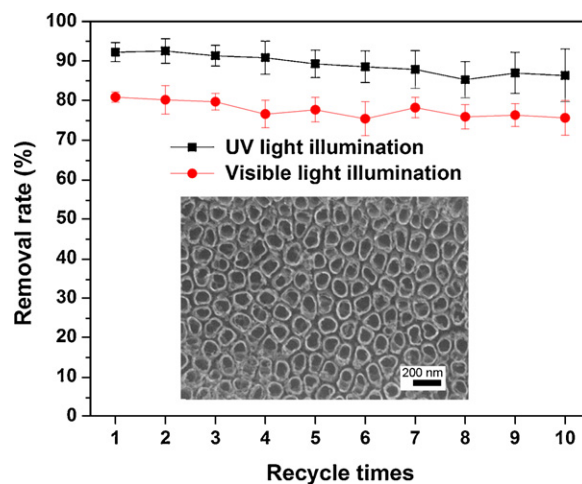
heat treatment of TiO₂ nanotube soaked with high concentrated ammonia is a promising way to improve the efficiency of photocatalyst.

3.3. Comparison of photocatalytic activity

Fig. 7 demonstrates the kinetic behaviors of the MO photodegradation by the TiO₂ nanotube array catalyst calcined at different temperatures for 2 h under the high-pressure mercury lamp illumination. The MO photodegradation clearly obeyed the first-order reaction kinetics. The photolysis experiments, in the absence of TiO₂ photocatalyst, revealed that the self-degradation of MO was almost negligible under UV illumination. Table 1 shows the effect of annealing temperature of the TiO₂ nanotube array photocatalysts on the first-order rate constant *k* of photocatalytic degradation under different light sources. The apparent rate constant of photocatalytic degradation with the presence of TiO₂ nanotube photocatalyst was significantly higher than that of MO self-photofading under both light sources, indicating the TiO₂ play an important role in the photocatalytic process. From the plot of absorption vs. wavelength under different light source irradiation (Fig. 8), it can be seen that a rapid decrease in the absorbance peak at 508 nm reflects the degradation of MO on the N-doped TiO₂ nanotube array photocatalyst. The color removal of MO pollutant was almost completely in 15 min under high-pressure mercury light irradiation (Fig. 8(a)), and more than 80% under tungsten–halogen lamp illumination after 60 min (Fig. 8(b)). Under the high-pressure mercury lamp illumination, the photocatalytic degradation rate of MO initially increased with increasing of the annealing temperature of N-doped TiO₂ nanotube array film between 300 and 450 °C (0.071–0.169 min⁻¹), and then decreased. The optimized efficiency was obtained for the one annealed at 450 °C. This is attributed to the higher content in the crystalline anatase phase for the samples calcined at 450 °C than those at 300 and 600 °C. According to the XRD results, the phase transformation from amorphous TiO₂ to anatase was not incomplete at 300 °C. At 600 °C, some of anatase phase was transformed to the more stable but photocatalytically less active rutile phase. Moreover, the rapid TiO₂ crystallite growth

by sintering resulted in a thickening of tube walls, and decrease in surface area.

The photocatalytic process under tungsten–halogen lamp illumination has a similar trend in the reaction rate constant with that of high-pressure mercury lamp, except for the 450 °C heat treatment of pure TiO₂ nanotube sample. The apparent rate constant *k* increases from 0.0241 to 0.0270 min⁻¹ as the annealing temperature increases from 300 and 450 °C, and then decreases to 0.0200 min⁻¹ at 500 °C, indicating that the N-doped TiO₂ nanotube array films do have a good visible light photocatalytic activity. Although the larger percentage of anatase and has a better UV light photocatalytic activity (0.0967 min⁻¹), the visible light photocatalytic activity of 450 °C annealing pure TiO₂ sample (~0.0178 min⁻¹) is lower than that of N-doped TiO₂ nanotube array films calcined under 300 °C (0.0241 min⁻¹) by using tungsten–halogen lamp. This is ascribed to the fact that visible

**Fig. 9.** Recycling test of the N-doped TiO₂ nanotube arrays film on the MO removal rate under different light sources. The inset shows the SEM image of the N-doped TiO₂ nanotube arrays after ten repeated cycles test.

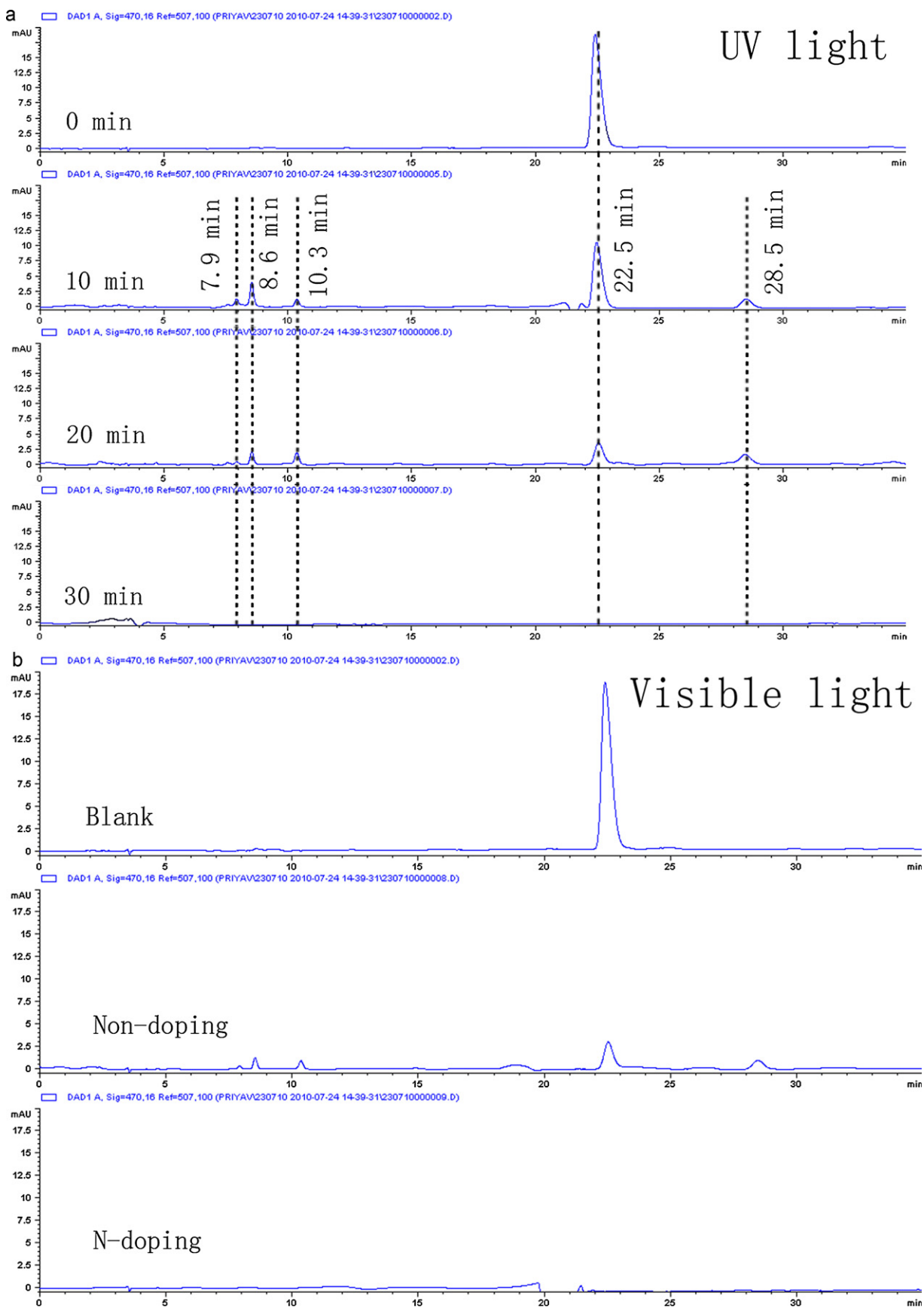


Fig. 10. HPLC profiles of methyl orange dye at different times during photocatalytic reaction under UV (a) or simulated solar lights (b) by the TiO₂ nanotube array photocatalyst with or without N-doping.

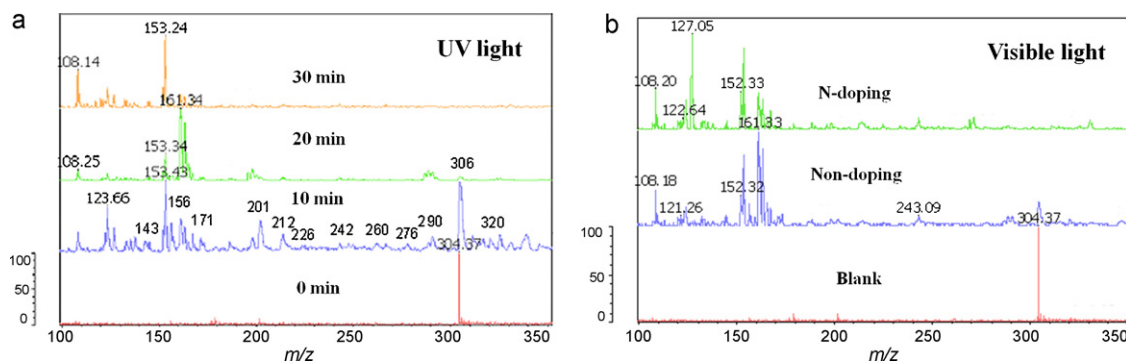


Fig. 11. MALDI-TOF mass spectrometry profiles of methyl orange and its oxidative intermediates corresponding to the solutions after being degraded under UV for different times (a) or simulated solar lights for 3 h (b) at pH 3.0.

light can more effectively excite the valence band electrons in the N-doped TiO_2 sample than pure TiO_2 sample. Therefore, the main contribution from visible light absorption has beneficial effect for the enhancement of photocatalytic activity.

Beside the excellent photocatalytic degradation performance, the N-doped TiO_2 nanotube arrays also show good stability of photocatalytic activity during the acidic liquid solution of MO. As shown in Fig. 9(a), the N-doped TiO_2 nanotube array structures kept without collapse and showed no apparent change in surface morphology after 10 cycles of repeat use in the photocatalytic process. In addition, the MO removal rate had only a slightly reduction within 8% under different light sources (Fig. 9(b)). However, the photocatalyst can recover its original activity as it was re-annealed at 450°C for 2 h. This may be due to the absorption of some intermediates not being fully removed during the photocatalytic experiment. These results indicated that the N-doped TiO_2 nanotube array film can remain active for long-term service without much degradation of its activity.

3.4. Preliminary discussion on degradation intermediates of methyl orange

The determination of intermediates and/or the photodegradation mechanism of azo dyes have been reported using GC/MS or

HPLC/MS techniques [61–65]. However, there are few studies on the intermediates and photodegradation pathway of the quinonoid MO (pH 3.0). Fig. 10(a) reports the chromatogram of the solution before and after photocatalytic degradation for different times. The intensity changes indicate the transversion of the degradation products. Before UV light irradiation, it can be seen that there exists only one peak corresponding to the MO with a negative ion at $m/z = 304$ and appeared at the retention time of 22.5 min in HPLC spectrum. After 10 min of UV light irradiation, the main absorption peak of MO decreased a lot and four additional fragment peaks corresponding to new main intermediate by-production initially appeared at $m/z = 320$ at 28.5 min, $m/z = 306$ at 10.3 min, $m/z = 290$ at 8.6 min and $m/z = 276$ at 7.9 min. Increasing the UV irradiation time, intermediate peaks gradually decreased except the peak at $m/z = 306$ at 10.3 min first increased but was still with low intensity at 20 min. At last, the peaks of methyl orange and intermediate products all almost disappear in HPLC after the 30 min UV irradiation, indicating that the photocatalytic degradation in the presence of anatase TiO_2 nanotube array can effectively mineralize many organic pollutants.

In the case of simulated solar light irradiation (Fig. 10(b)), the MO and intermediate peaks are eventually disappeared after 1 h photocatalytic reaction with the N-doped TiO_2 nanotube array catalyst. However, MO and main intermediate peaks were still

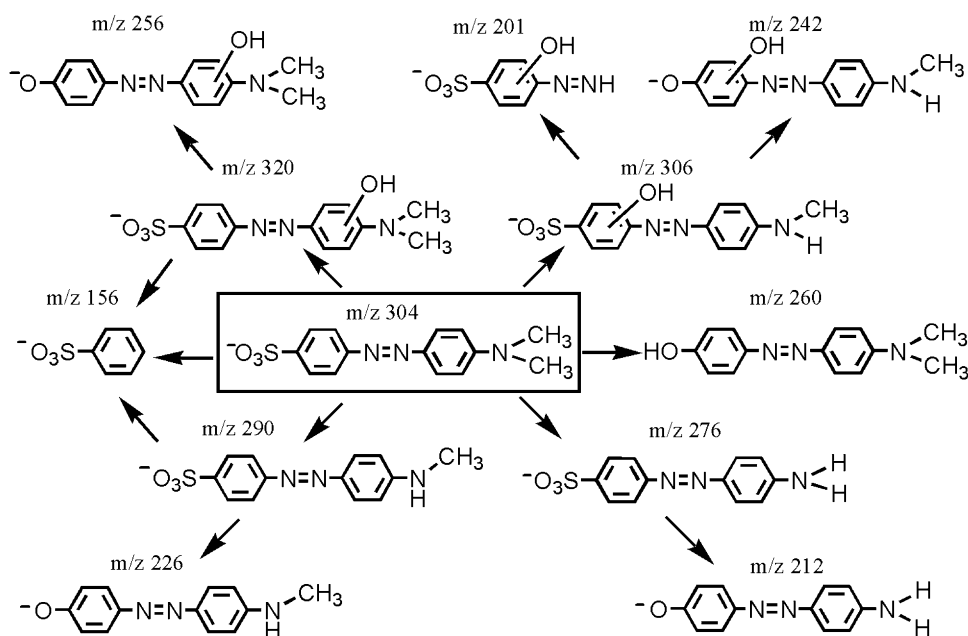


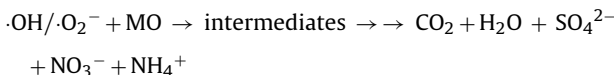
Fig. 12. Proposed degradation products and mechanism during the photodegradation process of MO.

observed with pure TiO₂ nanotube array catalyst under identical experimental conditions. Hence, under the artificial solar light, the MO dye showed a clearer trend to be degraded into low molecular weight byproducts by the photocatalyst with N-doping.

Fig. 11(a) shows the MALDI-TOF mass spectrometry profile recorded for MO solution after UV irradiation for different times. MO exhibited a clear MS signal corresponding to a negative ion of m/z 304. After 10 min UV irradiation, it is found that four new peaks (m/z = 320, 306, 290 and 276) are clear observed, indicating MO quickly changed to other chromophore groups. The compound of m/z = 320 is attributed to the monohydroxylated product of MO. The compound of m/z = 306 is the oxidation in the aromatic ring and loses one methyl group from nitrogen atom of amino group. The peak of m/z = 290 and 276 can be attributed to the loss of one or two methyl groups from MO (see Fig. 12).

Further increasing the irradiation time, these chromophore groups can decompose to lower molecular weight by-production by the attack of oxidative species ($\cdot\text{OH}$ and $\cdot\text{O}_2^-$) through two primary processes of dealkylation and hydroxylation. The compound of m/z = 320 yields the intermediate by-products corresponding to $[\text{M}-\text{H}-\text{SO}_2]^-$ at m/z = 256 and $[\text{M}-\text{H}-\text{N}_2\text{C}_6\text{H}_3(\text{OH})\text{N}(\text{CH}_3)_2]^-$ at m/z = 156. The compound of m/z = 306 yields the intermediate by-products corresponding to $[\text{M}-\text{H}-\text{SO}_2]^-$ at m/z = 242 and $[\text{M}-\text{H}-\text{N}_2\text{C}_6\text{H}_3(\text{OH})\text{NHCH}_3]^-$ at m/z = 156. The compound of m/z = 290 yields the intermediate by-products corresponding to $[\text{M}-\text{H}-\text{SO}_2]^-$ at m/z = 226, $[\text{M}-\text{H}-\text{CH}_3]^-$ at m/z = 275 and $[\text{M}-\text{H}-\text{N}_2\text{C}_6\text{H}_4\text{NHCH}_3]^-$ at m/z = 156. The compound of m/z = 276 yields the intermediate by-products corresponding to $[\text{M}-\text{H}-\text{SO}_2]^-$ at m/z = 212, and $[\text{M}-\text{H}-\text{N}_2\text{C}_6\text{H}_4\text{NH}_2]^-$ at m/z = 156.

Finally, the photogenerated oxidative species forming over TiO₂ nanotube array catalyst surface further decompose these intermediates to the final carbon dioxide and some non-toxic inorganic products (SO_4^{2-} , NO_3^- and NH_4^+) as shown in following equation:



The MS results (Fig. 11(b)) of MO solution by TiO₂ nanotube array catalyst with or without N-doping under tungsten-halogen lamp irradiation for 3 h showed that the N-doped photocatalyst exhibits better visible light activity than pure TiO₂ nanotube array to mineralize parent pollutant into non-toxic inorganic molecular.

On the basis of the preceding experimental results, we propose the four main intermediates were found during the initial photocatalytic degradation process of quinonoid MO followed by decomposing into smaller molecular weight by-products and finally mineralized. The possible degradation pathway of quinonoid MO is shown in Fig. 12. In addition, there were other fragment ions engendered in the degradation process which were not showed here. Those peaks were at m/z = 171 and 143. N-doped TiO₂ nanotube array catalyst shows enhanced photocatalytic activity than pure TiO₂ nanotube array catalyst to mineralize MO into non-toxic inorganic products under both high-pressure mercury lamp and tungsten-halogen lamp irradiation.

4. Conclusions

A simple method was developed for the fabrication of highly visible light active and stable nanocrystalline N-doped TiO₂ photocatalysts by ambient heat treatment of the TiO₂ nanotube array film pre-soaked in ammonia solution. The effect of annealing temperature on the photocatalytic activity of pure TiO₂ nanotube array films and N-doped TiO₂ nanotube array films under UV or visible light sources were investigated. It was found that photocatalytic activity of N-doped TiO₂ array strongly depended on the calcination temperature and the light source used for the degrada-

tion experiment. The N-doped TiO₂ array films calcined at 450 °C have the highest photocatalytic activity to degrade MO pollutant under visible (0.027 min⁻¹) or UV light (0.169 min⁻¹) sources. With combined advantages of large absorption area of the nanotube structures and the extended light absorption of N-doping, N-doped TiO₂ nanotube arrays shows good potential for sustainably photocatalytic degradation of environmental hazardous substances.

Acknowledgments

The authors thank the National Research Foundation of the Singapore Government (Grant MEWR651/06/160), the National Nature Science Foundation of China (20773100, 51072170, 21021002) and National Basic Research Program of China (973 Program) (2007CB935603).

References

- [1] A. Fujishima, K. Honda, Electrochemical photolysis of water at a semiconductor electrode, *Nature* 238 (1972) 37–39.
- [2] G.K. Mor, S.G. Shankar, M. Paulose, O.K. Varghese, C.A. Grimes, Use of highly-ordered TiO₂ nanotube arrays in dye-sensitized solar cells, *Nano Lett.* 6 (2006) 215–218.
- [3] K.G. Ong, O.K. Varghese, G.K. Mor, K. Shankar, C.A. Grimes, Application of finite-difference time domain to dye-sensitized solar cells: the effect of nanotube-array negative electrode dimensions on light absorption, *Sol. Energy Mater. Sol. Cells* 91 (2007) 250–257.
- [4] J.M. Macak, M. Zlamal, J. Krysta, P. Schmuki, Self-organized TiO₂ nanotube layers as highly efficient photocatalysts, *Small* 3 (2007) 300–304.
- [5] X. Quan, S.G. Yang, X.L. Ruan, H.M. Zhao, Preparation of titania nanotubes and their environmental applications as electrode, *Environ. Sci. Technol.* 39 (2005) 3770–3775.
- [6] Y.K. Lai, L. Sun, Y.C. Chen, H.F. Zhuang, C.J. Lin, J.W. Chin, Effects of the structure of TiO₂ nanotube array on Ti substrate on its photocatalytic activity, *J. Electrochem. Soc.* 153 (2006) D123–D127.
- [7] M. Paulose, G.K. Mor, O.K. Varghese, K. Shankar, C.A. Grimes, Visible light photoelectrochemical and water-photoelectrolysis properties of titania nanotube arrays, *J. Photochem. Photobiol. A: Chem.* 178 (2006) 8–15.
- [8] G.K. Mor, K. Shankar, M. Paulose, O.K. Varghese, C.A. Grimes, Enhanced photocleavage of water using titania nanotube arrays, *Nano Lett.* 5 (2005) 191–195.
- [9] O.K. Varghese, D.W. Gong, M. Paulose, K.G. Ong, E.C. Dickey, C.A. Grimes, Extreme changes in the electrical resistance of titania nanotubes with hydrogen exposure, *Adv. Mater.* 15 (2003) 624–627.
- [10] O.K. Varghese, G.K. Mor, C.A. Grimes, M. Paulose, N. Mukherjee, A titania nanotube-array room-temperature sensor for selective detection of hydrogen at low concentrations, *J. Nanosci. Nanotech.* 4 (2004) 733–737.
- [11] S.C. Roy, M. Paulose, C.A. Grimes, The effect of TiO₂ nanotubes in the enhancement of blood clotting for the control of hemorrhage, *Biomaterials* 28 (2007) 4667–4672.
- [12] B.C. Yang, M. Uchida, H.M. Kim, X.D. Zhang, T. Kokubo, Preparation of bioactive titanium metal via anodic oxidation treatment, *Biomaterials* 25 (2004) 1003–1010.
- [13] M. Anpo, S. Dohshi, M. Kitano, Y. Hu, M. Takeuchi, M. Matsuoka, The preparation and characterization of highly efficient titanium oxide-based photofunctional materials, *Ann. Rev. Mater. Res.* 35 (2005) 1–27.
- [14] N. Serpone, Is the band gap of pristine TiO₂ narrowed by anion- and cation-doping of titanium dioxide in second-generation photocatalysts? *J. Phys. Chem. B* 110 (2006) 24287–24293.
- [15] J.G. Yu, Q.J. Xiang, M.H. Zhou, Preparation, characterization and visible-light-driven photocatalytic activity of Fe-doped titania nanorods and first-principles study for electronic structures, *Appl. Catal. B: Environ.* 90 (2009) 595–602.
- [16] L.X. Yang, D.M. He, Q.Y. Cai, C.A. Grimes, Fabrication and catalytic properties of Co-Ag-Pt nanoparticle-decorated titania nanotube arrays, *J. Phys. Chem. C* 111 (2007) 8214–8217.
- [17] J.M. Macak, F. Schmid-Stein, P. Schmuki, Efficient oxygen reduction on layers of ordered TiO₂ nanotubes loaded with Au nanoparticles, *Electrochem. Commun.* 9 (2007) 1783–1787.
- [18] A. Orlov, D.A. Jefferson, N. Macleod, R.M. Lambert, Photocatalytic properties of TiO₂ modified with gold nanoparticles in the degradation of 4-chlorophenol in aqueous solution, *Catal. Lett.* 92 (2004) 41–47.
- [19] L. Sun, J. Li, C.L. Wang, S.F. Li, Y.K. Lai, H.B. Chen, C.J. Lin, Ultrasound aided photochemical synthesis of Ag loaded TiO₂ nanotube arrays to enhance photocatalytic activity, *J. Hazard. Mater.* 171 (2009) 1045–1050.
- [20] R. Asahi, T. Ohwaki, K. Aoki, Y. Taga, Visible-light photocatalysis in nitrogen-doped titanium oxides, *Science* 293 (2001) 269–271.
- [21] T. Ohno, M. Akiyoshi, T. Umabayashi, K. Asai, T. Mitsui, M. Matsumura, Preparation of S-doped TiO₂ photocatalysts and their photocatalytic activities under visible light, *Appl. Catal. A: Gen.* 265 (2004) 115–121.

- [22] T. Ohno, T. Mitsui, M. Matsumura, Photocatalytic activity of S-doped TiO₂ photocatalyst under visible light, *Chem. Lett.* 32 (2003) 364–365.
- [23] B. Kosowska, S. Mozia, A.W. Morawski, B. Grzmil, M. Janus, K. Kalucki, The preparation of TiO₂-nitrogen doped by calcinations of TiO₂·xH₂O under ammonia atmosphere for visible light photocatalysis, *Sol. Cells* 88 (2005) 269–280.
- [24] M. Janus, J. Choina, A.W. Morawski, Azo dyes decomposition on new nitrogen-modified anatase TiO₂ with high adsorptivity, *J. Hazard. Mater.* 166 (2009) 1–5.
- [25] K.L. Lv, J.G. Yu, K.J. Deng, J. Sun, Y.X. Zhao, D.Y. Du, M. Li, Synergistic effects of hollow structure and surface fluorination on the photocatalytic activity of titania, *J. Hazard. Mater.* 173 (2010) 539–543.
- [26] M.H. Zhou, J.G. Yu, Preparation and enhanced daylight-induced photocatalytic activity of C,N,S-tridoped titanium dioxide powders, *J. Hazard. Mater.* 152 (2008) 1229–1236.
- [27] J.H. Xu, W.L. Dai, J.X. Li, Y. Cao, H.X. Li, H.Y. He, K.N. Fan, Simple fabrication of thermally stable apertured N-doped TiO₂ microtubes as a highly efficient photocatalyst under visible light irradiation, *Catal. Commun.* 9 (2008) 146–152.
- [28] Y.W. Wang, Y. Huang, W.K. Ho, L.Z. Zhang, Z.G. Zou, S.C. Lee, Biomolecule-controlled hydrothermal synthesis of C-N-S-tridoped TiO₂ nanocrystalline photocatalysts for NO removal under simulated solar light irradiation, *J. Hazard. Mater.* 169 (2009) 77–87.
- [29] Y. Mizukoshi, N. Ohtsu, S. Semboshi, N. Masahashi, Visible light responses of sulfur-doped rutile titanium dioxide photocatalysts fabricated by anodic oxidation, *Appl. Catal. B: Environ.* 91 (2009) 152–156.
- [30] C.X. Feng, Y. Wang, Z.S. Jin, J.W. Zhang, S.L. Zhang, Z.S. Wu, Z.J. Zhang, Photoactive centers responsible for visible-light photoactivity of N-doped TiO₂, *New J. Chem.* 32 (2008) 1038–1047.
- [31] O. Diwald, T.L. Thompson, E.G. Goralski, S.D. Walck, J.T. Yates, The effect of nitrogen ion implantation on the photoactivity of TiO₂ rutile single crystals, *J. Phys. Chem. B* 108 (2004) 52–57.
- [32] T. Lindgren, J.M. Mwabora, E. Avendan, J. Jonsson, A. Hoel, G. Granqvist, S. Lindquist, Photoelectrochemical and optical properties of nitrogen doped titanium dioxide films prepared by reactive DC magnetron sputtering, *J. Phys. Chem. B* 107 (2003) 5709–5716.
- [33] H. Irie, Y. Watanabe, K. Hashimoto, Nitrogen-concentration dependence on photocatalytic activity of TiO_{2-x}N_x powders, *J. Phys. Chem. B* 107 (2003) 5483–5486.
- [34] R. Nakamura, T. Tanaka, Y. Nakatio, Mechanism for visible light responses in anodic photocurrents at N-doped TiO₂ film electrodes, *J. Phys. Chem. B* 108 (2004) 10617–10620.
- [35] Y. Wang, C.X. Feng, Z.S. Jin, J.W. Zhang, J.J. Yang, S.L. Zhang, A novel N-doped TiO₂ with high visible light photocatalytic activity, *J. Mol. Catal. A: Chem.* 260 (2006) 1–3.
- [36] L. Dong, G.X. Cao, Y. Ma, X.L. Jia, G.T. Ye, S.K. Guan, Enhanced photocatalytic degradation properties of nitrogen-doped titania nanotube arrays, *Trans. Non-ferrous Met. Soc. China* 19 (2009) 1583–1587.
- [37] G. Liu, F. Li, D.W. Wang, D.M. Tang, C. Liu, X.L. Ma, G.Q. Lu, H.M. Cheng, Electron field emission of a nitrogen-doped TiO₂ nanotube array, *Nanotechnology* 19 (2008) 025606.
- [38] A. Ghicov, J.M. Macak, H. Tsuchiya, J. Kunze, V. Haeublein, S. Kleber, P. Schmuki, TiO₂ nanotube layers: dose effects during nitrogen doping by ion implantation, *Chem. Phys. Lett.* 419 (2006) 426–429.
- [39] A. Ghicov, J.M. Macak, H. Tsuchiya, J. Kunze, V. Haeublein, L. Frey, P. Schmuki, Ion implantation and annealing for an efficient N-doping of TiO₂ nanotubes, *Nano Lett.* 6 (2006) 1080–1082.
- [40] T. Ihara, M. Miyoshi, Y. Iriyama, O. Matsumoto, S. Sugihara, Visible-light-active titanium oxide photocatalyst realized by an oxygen-deficient structure and by nitrogen doping, *Appl. Catal. B: Environ.* 42 (2003) 403–409.
- [41] Z.P. Wang, W.M. Cai, X.T. Hong, X.L. Zhao, F. Xu, C.G. Cai, Photocatalytic degradation of phenol in aqueous nitrogen-doped TiO₂ suspensions with various light sources, *Appl. Catal. B: Environ.* 57 (2005) 223–231.
- [42] Y.K. Lai, X.F. Gao, H.F. Zhuang, J.Y. Huang, C.J. Lin, L. Jiang, Designing Superhydrophobic porous nanostructures with tunable water adhesion, *Adv. Mater.* 21 (2009) 3799–3803.
- [43] Y.K. Lai, C.J. Lin, H. Wang, J.Y. Huang, H.F. Zhuang, L. Sun, Superhydrophilic-superhydrophobic micropattern on TiO₂ nanotube films by photocatalytic lithography, *Electrochem. Commun.* 10 (2008) 387–391.
- [44] H.F. Zhuang, C.J. Lin, Y.K. Lai, L. Sun, J. Li, Some critical structure factors of titanium oxide nanotube array in its photocatalytic activity, *Environ. Sci. Technol.* 41 (2007) 4735–4740.
- [45] Y.K. Lai, H.F. Zhuang, L. Sun, Z. Chen, C.J. Lin, Self-organized TiO₂ nanotubes in mixed organic-inorganic electrolytes and their photoelectrochemical performance, *Electrochim. Acta* 54 (2009) 6536–6542.
- [46] J.G. Yu, B. Wang, Effect of calcination temperature on morphology and photoelectrochemical properties of anodized titanium dioxide nanotube arrays, *Appl. Catal. B: Environ.* 94 (2010) 295–302.
- [47] O.K. Varghese, D.W. Gong, M. Paulose, C.A. Grimes, E.C. Dickey, Crystallization and high-temperature structural stability of titanium oxide nanotube arrays, *J. Mater. Res.* 18 (2003) 156–165.
- [48] H.Z. Zhang, J.F. Banfield, Phase transformation of nanocrystalline anatase-to-rutile via combined interface and surface nucleation, *J. Mater. Res.* 15 (2000) 437–448.
- [49] Y.K. Lai, C.J. Lin, J.Y. Huang, H.F. Zhuang, L. Sun, T. Nguyen, Markedly controllable adhesion of superhydrophobic sponglike nanostructure TiO₂ films, *Langmuir* 24 (2008) 3867–3873.
- [50] Y.K. Lai, Z.Q. Lin, J.Y. Huang, L. Sun, Z. Chen, C.J. Lin, Controllable construction of ZnO/TiO₂ patterning nanostructures by superhydrophilic/superhydrophobic templates, *New J. Chem.* 34 (2010) 44–51.
- [51] M. Sathish, B. Viswanathan, R.P. Viswanath, Characterization, photocatalytic activity of N-doped TiO₂ prepared by thermal decomposition of Ti-melamine complex, *Appl. Catal. B: Environ.* 74 (2007) 307–312.
- [52] Y.N. Huo, Y. Jin, J. Zhu, H.X. Li, Highly active TiO_{2-x}N_xF_y visible photocatalyst prepared under supercritical conditions in NH₄F/EtOH fluid, *Appl. Catal. B: Environ.* 89 (2009) 543–550.
- [53] T. Osaki, K. Nagashima, K. Watari, K. Tajiri, Silica-doped alumina cryogels with high thermal stability, *J. Non-Cryst. Solids* 353 (2007) 2436–2442.
- [54] Y.P. Yu, X.J. Xing, L.M. Xu, S.X. Wu, S.W. Li, N-derived signals in the X-ray photoelectron spectra of N-doped anatase TiO₂, *J. Appl. Phys.* 105 (2009) 123535.
- [55] D.W. Bahnemann, R. Dillert, P.K.J. Robertson, *Chemical Physics of Nanostructured Semiconductors*, XSP BV, Eindhoven, 2003.
- [56] Y.K. Lai, L. Sun, C. Chen, C.G. Nie, J. Zuo, C.J. Lin, Optical and electrical characterization of TiO₂ nanotube arrays on titanium substrate, *Appl. Surf. Sci.* 252 (2005) 1101–1106.
- [57] G. Ramis, G. Busca, C. Cristiani, L. Lietti, P. Forzatti, F. Bregani, Characterization of tungsta titania catalysts, *Langmuir* 8 (1992) 1744–1749.
- [58] S.D. Mo, W.Y. Ching, Electronic and optical-properties of 3 phase of titanium-dioxide-rutile, anatase, and brookite, *Phys. Rev. B* 51 (1995) 13023–13031.
- [59] D. Mardare, G.I. Rusu, The influence of heat treatment on the optical properties of titanium oxide thin films, *Mater. Lett.* 56 (2002) 210–214.
- [60] R. Beranek, H. Tsuchiya, T. Sugishima, J.M. Macak, L. Taveira, S. Fujimoto, H. Kisch, P. Schmuki, Enhancement and limits of the photoelectrochemical response from anodic TiO₂ nanotubes, *Appl. Phys. Lett.* 87 (2005) 243114.
- [61] C. Baiocchi, M.C. Brussino, E. Pramauro, A.B. Prevot, L. Palmisano, G. Marci, Characterization of methyl orange and its photocatalytic degradation products by HPLC/UV–VIS diode array and atmospheric pressure ionization quadrupole ion trap mass spectrometry, *Int. J. Mass Spectrom.* 214 (2002) 247–256.
- [62] T.W. Chen, Y.H. Zheng, J.M. Lin, G.N. Chen, Study on the photocatalytic degradation of methyl orange in water using Ag/ZnO as catalyst by liquid chromatography electrospray ionization ion-trap mass spectrometry, *J. Am. Soc. Mass Spectrom.* 19 (2008) 997–1003.
- [63] H. Han, R.B. Bai, Highly effective buoyant photocatalyst prepared with a novel layered-TiO₂ configuration on polypropylene fabric and the degradation performance for methyl orange dye under UV–Vis and Vis lights, *Sep. Purif. Technol.* 73 (2010) 142–150.
- [64] W.J. Li, D.Z. Li, W.J. Zhang, Y. Hu, Y.H. He, X.Z. Fu, Microwave synthesis of Zn_xCd_{1-x}S nanorods and their photocatalytic activity under visible light, *J. Phys. Chem. C* 114 (2010) 2154–2159.
- [65] A.K.L. Sajjad, S. Shamaila, B.Z. Tian, F. Chen, J.L. Zhang, Comparative studies of operational parameters of degradation of azo dyes in visible light by highly efficient WO₃/TiO₂ photocatalyst, *J. Hazard. Mater.* 177 (2010) 781–791.